

GEOPHYSICS[®]

EXPERIMENTAL STUDY OF TEMPERATURE CHANGE EFFECT ON DAS CONTINUOUS MEASUREMENTS.

Journal:	<i>Geophysics</i>
Manuscript ID	GEO-2021-0524.R2
Manuscript Type:	Technical Paper
Keywords:	DAS (distributed acoustic sensors), borehole geophysics, monitoring, field experiments, passive seismic
Manuscript Focus Area:	Borehole Geophysics, Passive Seismic and Microseismic Methods

SCHOLARONE™
Manuscripts

**EXPERIMENTAL STUDY OF TEMPERATURE CHANGE EFFECT ON DAS
CONTINUOUS MEASUREMENTS**

Evgenii Sidenko^{1,2} (evgenysidenko@gmail.com)

Konstantin Tertyshnikov^{1,2} (Konstantin.Tertyshnikov@curtin.edu.au)

Maxim Lebedev^{1,2} (M.Lebedev@exchange.curtin.edu.au)

Roman Pevzner^{1,2} (R.Pevzner@curtin.edu.au)

¹Curtin University, Perth, Western Australia

²CO2CRC Ltd., Australia

Right Running Head: Temperature change effect on DAS measurements

Corresponding author: Evgenii Sidenko - evgenysidenko@gmail.com

Address: Exploration Geophysics, Curtin University, 26 Dick Perry Ave, Kensington,

WA, 6151, Australia

ABSTRACT

Distributed fiber-optic sensing is useful in geophysical exploration and monitoring applications. Distributed temperature sensing (DTS) is used for measuring and monitoring temperature and distributed acoustic sensing (DAS) for recording the seismic wavefield. However, DAS measurements are also sensitive to temperature changes. To understand and quantify the DAS signature of temperature changes during water injections at CO2CRC Otway site, a series of experiments were conducted at the Curtin/NGL well research facility and Curtin Rock-Physics Laboratory. Overall, three DAS cables were examined. Two fibers were tested in the laboratory and one cable, which is installed behind the casing in the Curtin/NGL well, was examined in the well. Laboratory measurements and observations made during analysis of passive DAS and DTS field data recorded in four Otway wells demonstrate that DAS is sensitive to long-period temperature changes and its response is proportional to the time derivative of temperature. Induced fiber strain is linearly related to slow temperature change and this dependency can be estimated for a particular cable. Obtained proportionality constants between strain and temperature change show some dependency on the cable type/design and acquisition setup, but are all of the same order of magnitude. DAS measurements can also be affected by

low-frequency noise possibly associated with the effect of temperature on the DAS acquisition unit itself. The results can help compensate for the effect of temperature on low-frequency DAS signal and show that DAS can be used as a distributed temperature sensor if direct temperature measurements are not available.

INTRODUCTION

Fiber-optic distributed acoustic sensing (DAS) is an emerging technology, which has already found a widespread application in seismic acquisition and reservoir monitoring (Mateeva et al., 2014; Karrenbach et al., 2019; Isaenkov et al., 2021). DAS measurements can be affected by temperature variations caused by both natural and industrial processes such as diurnal atmospheric temperature variations, hydraulic fracturing treatments (Bakku* et al., 2014; Karrenbach et al., 2017, 2019), borehole fluids flows (Sharma et al., 2020; Titov et al., 2020) or temperature variations in geothermal reservoirs (Miller and Coleman, 2018). Such temperature variations can be considered as a low-frequency signal (< 0.1 Hz). This frequency range is far below typical frequencies utilized in seismic exploration. However, DAS applications often include passive broadband monitoring of the subsurface. Since fiber-optic measurements are

capable of acquiring data at very low frequencies, passive DAS recording is often used to study natural phenomena at frequencies far below 1 Hz such as distant earthquakes (Ajo-Franklin et al., 2019), oceanic microseisms (Lindsey et al., 2019; Glubokovskikh et al., 2021), earth tides (Becker and Coleman, 2019). Low-frequency DAS is also being utilised in different industrial applications, such as hydraulic fractures geometry characterisation (Jin and Roy, 2017), low-frequency strain measurements (Becker et al., 2019), multiphase flow characterisation (Titov et al., 2020; Sharma et al., 2021), wellbore gas influx detection (Feo et al., 2020; Sharma et al., 2021), fluid pressure sensing (Becker et al., 2017), monitoring of well integrity (Raab et al., 2019) and borehole decommissioning operations (Ricard et al., 2019). Since temperature variations can occur in the same frequency band, they can distort low-frequency seismic records.

Understanding the effect of temperature changes on the strain rate measured by DAS can help to compensate for this effect in the data. However, the temperature response on DAS should not be always treated as noise. In some situations, for example, when there is no separate temperature measurements, such as distributed temperature sensing (DTS), DAS can be utilized for relative temperature monitoring as well (Koyamada et al., 2009; Bao and Wang, 2021).

There are two main aspects of how DAS amplitudes can be affected by the temperature change: thermal expansion and refractive index change (thermo-optic effect). Phase-based DAS interrogators measure the phase difference of the backscattered light. From Bakku (2015) and Fang (2012), amplitude dependence on temperature change can be expressed as:

$$\Delta\Phi = \Phi\Delta T(\alpha_T + \xi)$$

where $\Delta\Phi$ is the amplitude of the DAS signal (change of optical phase); Φ the optical phase; ΔT the temperature change; α_T the thermal expansion coefficient; ξ the thermo-optic effect coefficient. Thermal expansion effect manifests itself as an induced strain, while thermo-optic effect changes the refractive index of the fiber. Both of these phenomena have the same effect on DAS measurements as they both change the travel time of the laser pulse in the fiber. For a silica fiber, the thermal expansion coefficient is $0.5 \cdot 10^{-6} \text{ }^\circ\text{C}^{-1}$ (Roy et al., 1989; Feng et al., 2010) and the thermo-optic coefficient is $\sim 0.68 \cdot 10^{-5} \text{ }^\circ\text{C}^{-1}$ (Palik, 1997; Adamovsky et al., 2012; Gao et al., 2018). These values demonstrate that the temperature effect on DAS is mainly defined by the change of the refractive index (thermo-optic effect). However, different cable designs and ways of cable deployment can behave differently under changing thermal conditions as different

materials and compositions will expand/compress differently in response to temperature changes. Thus, DAS response to the changing temperature is likely to depend on a particular cable setup.

In order to study the temperature effect on DAS in a controlled environment, we first run series of experiments in Curtin/NGL well and Curtin's rock-physics laboratory. First, in order to estimate the order of the temperature effect on DAS measurements in the seismically quiet environment (borehole) we conducted the experiment in a research well on the Curtin University Campus. Then, to study temperature response on different cables, we conducted an experiment at the Curtin Rock-Physics Laboratory where we organised a heating/cooling setup which allowed us to control the temperature variations. The findings of these controlled experiments are then applied to multi-well DAS observations during water injections performed as part of the Otway CO2 Geosequestration Project. Overall, two different fibers were tested in the laboratory and one cable, which is installed behind the casing in the Curtin/NGL well, was examined at the research facility site. After that, we analysed passive DAS and DTS field data recorded during water injections within the Otway CO2 geosequestration project.

All experiments show that DAS is sensitive to long-period temperature changes and its strain-rate is proportional to the time derivative of temperature. All our tests show a linear dependency of DAS strain-rate response to the temperature time derivative. However, our results show that different cables and different installation designs behave differently under the changing temperature conditions.

Using the linear trend estimated from the data, temperature effect on DAS measurements can be predicted and separated from signals related to purely mechanical deformations. However, different DAS acquisition setups can have different responses to the changing temperature and should be calibrated/tested separately. Also, our study reveals possible low-frequency equipment-related noise that should be removed from data before low-frequency signal analysis.

BOREHOLE EXPERIMENT: CURTIN/NGL RESEARCH FACILITY

Data acquisition

For the borehole experiment, we acquired data at the Curtin/NGL research facility located at Curtin University main campus in Perth, Western Australia. We utilized an iDASv2

(Silixa Ltd) interrogator and BandWeaver DTS (Bandweaver) connected to a fiber-optic (FO) cable cemented behind the casing of the 900 m deep Curtin/NGL well. The cemented fiber-optic cable is a non-metallic armoured loose-tube cable carrying single and multimode fibers, which are housed in individual plastic buffer tubes filled with gel. Figure 1a shows the location of NGL well facility on the map. DTS and DAS units were placed in the NGL equipment room.

Figure 1b shows the schematic of the NGL well experiment. To explore the effect of a temperature change, we drop 50 kg of ice into the well. The ice stayed at a water level around 30 m deep. The ice melted and cooled the borehole water, which caused the temperature decrease of the well's casing and the fiber-optic cable cemented behind it. Figure 2 shows the DTS and DAS data recorded during this experiment. Figures 2a and 2b show four days of DTS data and its time derivative. DTS recording uses 1 m channel spacing. Figure 2c shows 24 hours of DAS data decimated to 5 m channel spacing. The vertical dotted black lines in Figures 2a and 2b indicate the start and end times of the DTS record shown in Figures 2c. The temperature anomaly is clearly visible on both DTS and DAS data recorded on 07/08/2020 at the same depth level around 25-30 m.

DTS data are shown in Figure 2a as a temperature change with respect to the baseline (ambient temperature distribution) temperature. Both DAS and DTS data in Figure 2 are shown after subtraction of a background trend related to diurnal temperature changes in the room housing the acquisition unit (as described in the next chapter). The response from the introduced ice can be traced on DTS data over 2 to 3 days. DAS measurements demonstrate a shorter visible response of only ~3-4 hours. From Figure 2 it is clear that the DAS response corresponds to the temperature derivative. This happens because DTS measures the temperature along the fiber while DAS measures the strain rate, which is proportional to the time derivative of temperature. Thus, DAS primarily reacts to the temperature gradient.

Correction of measurements

Besides the signal related to the temperature change and high-frequency random noise, DAS and DTS recordings contain low-frequency periodic common-mode noise of unknown origin (shown with black arrows in Figure 3). It has been observed (e.g., Wang et al., 2018, Figure 3 and accompanying text) that DAS systems exhibit a small sensitivity to vibration of the interrogator that results in an easily estimated common signal present on all the DAS traces. It

seems that a similar sensitivity to environmental temperature changes occurs and can be remediated in the same way. The form of this noise, its consistency along the fiber, its periodicity and temporal coincidence on DAS and DTS suggest that it is most likely related to the changing ambient temperature conditions in the acquisition room housing both DAS and DTS interrogators. This temperature change signal can be attributed to the working regime of an air conditioning unit in the room.

To confirm this hypothesis, we ran a separate test in which we logged the temperature in the acquisition room over a few days with a portable temperature logger. The accuracy of the logger is 0.5 °C, which is enough to track the temperature trend in the acquisition room.

Comparison of the temperature logger data and continuous DAS record is presented in Figure 4.

Figure 4a shows the low-frequency DAS signal (strain rate) recorded with the fiber optic cable cemented in the well. It is clear that the DAS signal is changing with time, not with depth. Figure 4b shows the averaged DAS response along the 0 to 800 m depth interval in the well (black line) and logged room temperature (orange line). Comparison of the DAS strain-rate response and temperature log shows that the oscillation period of the temperature logger signal coincides with that of the low-frequency component of the DAS response, which suggests that they are of the

same origin. Positive DAS values correspond to the decreasing room's temperature, and vice versa (note that the ice in the borehole caused negative DAS values). Black and orange curves do not have to perfectly match each other as the DAS unit has its own built-in cooling system so the temperature inside the interrogator can differ from the ambient one. Nevertheless, this test indicates that the presented low-frequency common-mode signal in DAS and DTS recordings is not related to changing conditions in the borehole and should be filtered out or suppressed for further analysis.

To separate the signal of interest (response from the ice) from ambient-temperature related noise (common-mode noise), we estimated a noise trace for both DAS and DTS by averaging the recorded data over the depth range of 600-800 m. Figure 5 shows DAS data before (a,b) and after (c) common-mode noise removal. Horizontal dashed lines in Figure 5a indicate the depth interval used to estimate the DAS common-mode noise. The estimated trace is then subtracted from the data. After the noise subtraction, only the signal related to the temperature change is observed on the traces from the 'ice' interval and no signal outside the 'ice' interval.

This calibration allowed us to highlight the response of DAS and DTS to the temperature change caused by the ice placed in the borehole. Figure 3 shows DAS and DTS recordings before and after noise subtraction for two different depths in the NGL well. Figure 3a and Figure 3c show DTS response at the depth of 26 m and 847 m; Figure 3b and Figure 3d show the DAS response at the same depth points. The depth of 26 m corresponds to the “ice” level; depth 847 m corresponds to the interval with no expected temperature change (signal should be constant for both DAS and DTS). All four plots (a,b,c,d) in Figure 3 present two traces: before and after acquisition noise removal. Black arrows in Figure 3 indicate the acquisition (room) noise. The amplitude of this noise in DAS data is comparable with the temperature response signal. DAS data is also complicated by strong “random” spikes that are related to vibrational (acoustic) signals. For DTS data, the level of the acquisition noise is significantly lower than the signal level. After removal of the acquisition noise, there is no visible signal at 847 m in both DAS and DTS data and at 26 m depth DAS and DTS signals are clearer.

Figure 6 shows the trace-to-trace comparison of DAS and DTS response at the “ice” level after data correction. Figure 6a shows DAS strain rate (black) and DTS time derivative (orange), Figure 6b shows DAS strain (black) and DTS (orange). The temperature strain-rate on DAS is

clearly evident and proportional to the temperature (DTS) time derivative. Figure 6b demonstrates an excellent match between strain and temperature. However, the calculated strain has some deviations caused by the integration of DAS data (strain rate) containing high amplitude spikes. Overall, both plots in Figure 6 suggest that there can be a linear relationship between two time series (strain and temperature change). Simultaneously obtained DAS and temperature recordings can be used to estimate DAS strain-rate response to the temperature change for a particular acquisition system as demonstrated below.

LABORATORY EXPERIMENT

To study the effect of changing temperature on DAS measurements in controlled temperature conditions, we designed a heating/cooling laboratory setup. We conducted a series of experiments in the Curtin Rock-Physics laboratory to estimate this effect as well as to gain insights on the influence of different fiber-optic cables on such temperature response. The laboratory setup is schematically shown in Figure 7.

We utilised the same iDASv2 interrogator (exactly the same unit as in the borehole experiment), a water bath coupled with a water heater/cooler, a temperature logger, testing fibers

(the fiber submerged in the water bath) and two pieces of reference fibers (coiled fiber connected before and after the water bath). The experiments were done with a bare single-mode fiber and a tight-buffered single-mode fiber. We used the coiled bare single-mode fiber as a reference fiber unaffected by water temperature (spliced to the testing fiber before and after the water bath).

Both experiments were conducted with several cycles of heating and cooling.

Figure 8 and Figure 9 show the results of the laboratory test with bare and tight-buffered fibers, respectively. Figure 8a and Figure 9a show the filtered (moving average smoothing) DAS strain-rate response for all DAS channels. White dashed lines outline margins between three pieces of coiled fibers shown in Figure 7 (two reference coils and a coil in the bath). DAS channels corresponding to the fiber in the water bath show a clear response to the temperature change: yellow colour indicates heating cycles; blue colour corresponds to cooling periods. The temperature logs are shown in orange colour in Figure 8c and Figure 9c, the time derivatives of temperature are shown in Figure 8b and Figure 9b (orange colour). Black curves in Figures 8b-c and Figures 9b-c correspond to averaged DAS responses (average trace computed for the channels between two black lines in Figure 8a and Figure 9a) and strain values calculated from DAS strain-rate amplitudes using integration, respectively.

In the bare fiber test, the DAS strain-rate response is very close to the temperature derivative (Figure 8b), while the strain calculated from the DAS strain rate looks similar to the temperature log (Figure 8c). These observations indicate a linear dependency between strain and temperature change. Results from the test with a tight-buffered fiber also demonstrate a good correspondence between DAS response and temperature change (Figure 9b-c). However, in the tight-buffered fiber test, the correlation between strain and temperature (or strain rate and temperature derivative) is not as strong as for the bare fiber. The estimated values of the Pearson correlation coefficient (Freedman et al., 2007) between the temperature time derivative (dT/dt) and DAS response (strain rate, $d\epsilon/dt$) are 0.975 for the bare fiber and 0.93 for the tight-buffered fiber. It seems that the presence of a tight coating in a cable design can cause deviation from linear strain-temperature dependence for a particular DAS-cable combination. To analyse this in more detail, later in the paper we estimate this dependency between strain and temperature change for both laboratory tests and for the borehole ice experiment.

WATER INJECTIONS AT THE OTWAY SITE

CO2CRC Otway Site

CO2CRC Otway Project is a pilot research project focused on the geological sequestration of CO₂ gas in a deep formation in the Australian State of Victoria (Cook, 2014). The current stage of the project is focused on borehole-based monitoring of a small (15 kt) injection of supercritical CO₂ into a saline aquifer through the CRC-3 well (Jenkins et al., 2017; Isaenkov et al., 2021). This vertical injection well and four slightly deviated monitoring wells (CRC-4, 5, 6, 7) are being used for seismic, temperature and pressure monitoring. Figure 10 shows the Otway site map with overlaid monitoring well trajectories. All five wells are equipped with fiber-optic sensing equipment: fiber-optic cables are cemented behind the casings and connected to DAS (Silixa Carina systems) and DTS (Silixa Ultima DTS) interrogators. A simplified schematic of fiber-optic cable deployment for the CRC-6 and CRC-7 wells is shown in Figure 11. The CRC-7 and CRC-6 wells share the same fiber-optic cable for DAS acquisition. Such acquisition design allows the use of a single DAS interrogator for two wells. The cable covers the CRC-7 well first (standard single-mode fiber downhole and engineering fiber uphole) and then CRC-6 (engineering fiber downhole only). DTS data is being acquired separately for both wells using a downhole-uphole cable loop design. Similarly to CRC-6 and CRC-7, CRC-4 and CRC-3 share the same DAS cable connected to the same interrogator (CRC-4 first, CRC-3

second). The cable that collects data from CRC-5 well is connected to another DAS unit which also records surface cable data (follows the CRC-5 well). Detailed description of the Otway project Stage-3 setup can be found in Isaenkov et al. (2021).

Both the CRC-6 and CRC-7 (as well as CRC-4 and CRC-5) wells are slightly deviated (not shown in Figure 11) from approximately 700 m measured depth (MD) to the bottom. The CRC-6 and CRC-7 wells are perforated around 1500 m MD and equipped with downhole pressure-temperature gauges installed above perforations. Pressure-temperature gauges are single point receivers and can be used as a reference for fiber-optic sensing data recorded at the same depth.

Water injections

The Otway monitoring design includes pressure tomography, which involves periodic water injections. The first series of water injections were performed in June-July 2020. Water was injected in all wells, except the CRC-3 well. During the injection, water from a surface water tank comes down a borehole and pushes the borehole fluid down along the well. As a result, the temperature is changing (decreasing) at each depth along the borehole due to the

borehole fluid (which is initially in thermal equilibrium with the surrounding rocks) being replaced with colder water from the surface. Examples of borehole pressure (black) and temperature (orange) variations recorded by borehole gauges are shown in Figures 12a-b. The temperature decrease can reach as much as 25°C. Pressure and temperature changes shown in Figures 12a-b clearly indicate the start and end of water injections in the CRC6 and CRC7 wells, respectively.

To examine the DAS strain-rate response to the temperature change, we extracted passive DAS data recorded in the CRC-6 and CRC-7 wells during the first water injection in July 2020. Figures 12c-d show spectral density calculated for both wells for a single DAS channel located right above the perforation interval. Corresponding borehole pressure and temperature gauge responses are shown in Figures 12a-b.

The spectrograms in Figure 12 shows the change of the frequency content in the range 0.008-10 Hz over time. The frequency band between 0.1 and 1-1.2 Hz contains mainly the signal from secondary oceanic microseisms (Bromirski, 2002; Nishida, 2017; Glubokovskikh et al., 2021). The dashed ellipses show the temperature response on DAS spectrograms during the

water injection in the CRC-6 well. The temperature response can be observed mainly in the frequency range below 0.1 Hz over the time interval that corresponds to the temperature change in the borehole. The cooling down process corresponds to the water injection (pump is on – the pressure is increasing), warming up process corresponds to the temperature equilibration process (pump is off – the pressure is returning back to its hydrostatic value). The low-frequency DAS response to the water injection occurs at the same time in both wells (highlighted by dashed ellipses). However, there is no evidence (Figure 12b) of temperature change in the CRC-7 well during injection in CRC-6 (and vice-versa). Thus, the anomaly in the adjacent CRC-7 well is artificial and can be explained with the measurement calibrations inside the DAS interrogator that acquires monitoring data from both the CRC-6 and CRC-7 wells simultaneously via the same cable. Besides the low-frequency temperature response, there are strong broadband events that can be mainly observed around the perforation interval and mostly in the injection well. These events can probably be treated as artefacts and could be caused by a direct (strong) temperature impact on the cemented fiber-optic cable. Injection in the CRC-7 well started 24 hours after the start of the water injection in the CRC-6 well. Similar to the first injection, there is a response in the data from both wells; broadband events are primarily associated with the

injector well. A few strong broadband events can be observed on the CRC-6 spectrogram during the injection in the CRC-7 well. However, those events are most likely associated with the previous injection in the CRC-6 well.

Joint DAS/DTS analysis and data calibration

In order to quantitatively estimate the relationship between DAS measurements and temperature for the water injection effect described in the previous section, we performed a time-domain analysis of DAS and DTS data recorded in the CRC-6 and CRC-7 wells. Figure 13 shows DAS and DTS data recorded during the water injection in the CRC-6 well. Figure 13a shows DTS data: the temperature change in the CRC-6 well. Figure 13b shows DAS data from the CRC-7 well. Figures 13c-d show DAS data from the CRC-6 well before and after correction respectively. All data in Figure 13 are shown after the removal of the high-frequency component using a moving average filter. Thus, here we are dealing only with low-frequency signals.

DTS data recorded in the CRC-6 well indicate a temperature decrease of more than 20°C (Figure 13a). This value matches the information recorded by the borehole temperature gauge in the well (Figures 12a). As water is being injected into the formation through the perforated

interval around 1500 m MD, there is no evidence of the temperature change below the perforated interval (only convectational heat exchange is possible). The start and stop of the water injection can be easily tracked on DTS data as a temperature decrease at 21:00 and an increase at 03:00.

As expected, CRC-6 DAS data (Figure 13c) recorded above the perforation depth correspond to temperature variations recorded by DTS. The DAS strain-rate signal responds to the time-derivative (rate of change) of the temperature. Thus, there is a clear change of polarity along the time vector when the temperature derivative changes the sign from negative to positive. Besides the temperature strain-rate response recorded by DAS, there are series of strong continuous periodic events that occur mainly around the perforation depth. These events correspond to broadband spikes on the DAS spectrogram (Figures 12c). They are most probably related to deformations of the cable or movements that can be caused either by slippage of the fiber core inside the gelled loose tube or by the cable relaxation due to strong direct impact of injected water on the cable at the perforation interval.

The signal on DAS below the perforation depth in the CRC-6 well perfectly repeats the CRC-7 DAS signal, which is uniform along the entire length of the well (Figure 13b). As there is

no evidence of temperature change either in the CRC-7 or CRC-6 well below the perforation, there should be no physical reason that could cause this effect on DAS measurements in the borehole (CRC-7). As such, this signal can be treated as an artificial acquisition noise. The existence of this noise in each well can be explained by the fact that DAS data in both wells are being recorded simultaneously by different parts of the single cable connected to a single interrogator (Figure 11). As most of the data in CRC-6 is dominated by the presence of the temperature signal, the observed artificial noise results from possible common-mode compensation inside the DAS unit. Nevertheless, this noise can be estimated for each time sample as a truncated mean value over the entire length of the CRC-7 well and then subtracted from the entire CRC-6 – CRC-7 dataset (Figure 13d). After the subtraction, there is no low-frequency signal related to the temperature change below the perforation interval.

Figure 14 shows an example of DAS and DTS data recorded during water injections in the CRC-5 well. Similarly to the injection in CRC-6, DTS shows no temperature change below the perforation interval (Figure 14a), the part of the DAS cable buried on the surface (outside the CRC-5 well) has a signal (Figure 14b) similar to CRC-5 below the perforation (Figure 14c).

After subtraction of the artificial noise estimated outside the injector well, the signal below perforation disappears (Figure 14d).

QUANTITATIVE DATA ANALYSIS

Simultaneously recorded temperature data (DTS or temperature logger) and DAS strain-rate data converted to strain (for all previously described acquisitions) allows us to estimate the overall coefficient for a particular fiber-optic cable or DAS acquisition setup for all previously described sets of data. To this end, we explore whether this coefficient differs between different cables depending on the installation design. In order to estimate thermal coefficients for all setups, we built cross-plots between strain estimated from DAS amplitudes and temperature change relative to the starting point (baseline value). Cross-plots for the NGL well and laboratory experiments are shown in Figure 15. To build these plots we took a single channel DAS data and temperature responses. Figure 15a shows the strain-temperature relation for the Curtin/NGL well experiment with ice dropped in the borehole; Figure 15b and c show results from the lab measurements with a bare fiber and tight-buffered fiber, respectively.

To estimate thermal coefficients (microstrain per degree Celsius) for the Curtin/NGL well experiment and laboratory test with the bare fiber, we used linear regression. Cross-plots for these two experiments clearly demonstrate the linear relationship between strain and temperature change. Estimated linear trends are shown in orange (Figure 15a) and green (Figure 15b) colours.

The estimated strain-temperature change coefficient for cable cemented in the NGL well is $2.9 \mu\epsilon/^\circ\text{C}$ and $9.1 \mu\epsilon/^\circ\text{C}$ for the bare fiber tested in the laboratory. Each coefficient represents the overall thermal effect for a particular tested cable. Both estimated coefficients are of the same order of magnitude. The estimated coefficient for the bare fiber is close to a thermo-optic coefficient of silica ($\frac{dn}{dT} = \xi * n_{eff} \approx 10^{-5} \text{ }^\circ\text{C}^{-1}$, where n_{eff} is the refractive index of silica). At the same time, it is not clear why the coefficient is lower for the fiber in a gel-fitted loose tube (cable in the well). A similar observation of a low apparent thermal coupling coefficient in a loose-tube optical cable was made by Miller and Coleman (2018). They suggested that the anomaly might be caused by the combined thermal response of the steel tube and its contents (gel and fiber). If the steel tube of the cable expands uniformly (both circumferentially and axially), to a greater extent than the gel, the result would be a volume deficit for the gel which could cause a net axial contracting force applied to the fibers inside.

The trend for the tight-buffered cable (Figure 15c) is not perfectly linear. Significantly different behavior can be observed from temperature-strain plots in Figures 8b-c and Figures 9b-c. Figures 8b-c shows a much clearer similarity between DAS and temperature time series. At the same time, the experiment with the tight-buffered fiber (Figures 9b-c) shows a clear deviation of DAS measurements from the temperature log for rapid heating/cooling intervals. Most likely, the deviation from the linear trend is caused by the presence of a tight coating (acrylate layer), which is firmly bound to the plastic fiber layer and experiences too rapid heating and cooling. Relatively fast temperature variations cause quite complicated interaction between the acrylate coating and the fiber itself due to the different thermal characteristics of these two materials (two orders of magnitude higher for acrylate than glass: 75 vs $0.55 \mu\epsilon/^\circ\text{C}$). Also, the thermal expansion coefficient and stiffness of plastic coating depend on the temperature. That can also cause non-linear dependence between strain and temperature change at low temperatures, as plastic becomes more stiff. Nevertheless, the right part of the cross-plot in Figure 15c shows linear behavior (blue line). The linear coefficient for this part is $10.5 \mu\epsilon/^\circ\text{C}$ which is slightly higher than the thermal coefficient obtained for the bare fiber ($9.1 \mu\epsilon/^\circ\text{C}$). The higher value for the tight-buffered fiber can be explained by the influence of the tight plastic

coating, which can result in a larger cumulative thermal effect. However, in the linear segments, the estimated values for both tested fibers are close and comparable to the thermo-optic coefficient for silica ($\approx 10 \mu\epsilon/^\circ\text{C}$).

Figure 16 shows cross-plots between DTS temperature change and DAS strain for four different injections (wells). Figures 16a-d show DAS-DTS values relationship before signal compensation and Figures 16e-h show corresponding data after the signal compensation. The cross-plots include data recorded at 10 m intervals from 100 to 1500 m MD (only above the perforation). Orange lines in Figure 16 show a linear regression estimated for each dataset. Estimated linear coefficients (slopes) correspond to the strain-temperature dependencies specific for each borehole setup.

Figures 16a-d demonstrate linear dependency between induced DAS response and temperature change. However, quite strong deviations from a linear trend can be observed for some depths (especially in Figure 16b and Figure 16d). Estimated strain-temperature coefficients change from $3.9 \mu\epsilon/^\circ\text{C}$ for the CRC-5 well to $7 \mu\epsilon/^\circ\text{C}$ for CRC-6 well.

Corrected data shown in Figures 16e-h demonstrate much clearer linearity between DAS and DTS and higher estimations for strain-temperature coefficients. Higher coefficients for the corrected data (Figures 16e-h) indicate that the applied signal compensation is a valid operation that helps to retrieve more accurate DAS measurements. Increased strain-temperature coefficients ($9.5 \mu\epsilon/^\circ\text{C}$ on average) are close to the estimation made in the laboratory experiment for a bare fiber (Figure 15b) despite different DAS interrogators used in these two studies.

CONCLUSIONS

To examine DAS strain-rate response and its sensitivity to changing temperature conditions, we performed three separate tests using the following setups: research NGL well with the fiber optic cable cemented behind the casing; controlled laboratory measurements with two different fibers and field borehole fiber-optic recordings of water injections in four wells at the Otway site. Phase based DAS is sensitive to temperature time derivative and is able to register very low-frequency signals (< 0.01 Hz). Our results demonstrate a linear relationship between DAS response and temperature change. The proportionality constant in these linear

relationships have different values for different types of DAS cables and installations but are all of the same order of magnitude (from 2.9 to 10.5 $\mu\epsilon/^\circ\text{C}$).

The rapid temperature change has a significant effect on DAS measurements and must be taken into account in time-lapse DAS seismic monitoring applications and especially in passive monitoring with the utilisation of low frequencies.

Knowing a linear dependency between strain and temperature we can potentially remove low-frequency temperature related noise from DAS data or use DAS records to estimate temperature variations along the fiber-optic cable. Thus, DAS can be potentially utilised to track temperature changes in the absence of DTS or other direct temperature measurements. However, utilisation of DAS and DTS together can be very beneficial, as it would allow estimating the thermal effect on DAS measurements and can help separate the temperature effect from the acoustic (seismic) signal.

The data analysis shows that DAS measurements can be affected by the artificial equipment-related noise that should be removed from data before low-frequency data analysis. It is caused by temperature variations in the room housing the acquisition unit and affects the

interrogator itself (shown in Curtin/NGL well experiment, iDASv2). This noise appears as a common-mode signal which is closely correlated with the room temperature. Similar equipment-related noise was observed during water injections in Otway (iDASv3). We observed weakened temperature signal for the cable section that was affected by the cold water and artificial signal for the section that was not affected by any temperature variation (adjacent borehole). Thus, this noise possibly appears because of internal measurements processing (common-mode subtraction). The described noise can be estimated using a reference (not affected by any signals) piece of fiber and subtracted from the data.

Many other aspects such as DAS acquisition parameters (gauge length and pulse length), types of interrogators, type of cable, cable installation designs, etc. influence the DAS measurements. Overall, it is apparent that the combination of a particular fiber optic cable, specific interrogator unit and deployment strategy should be considered, assessed and operated as a single acquisition system in which each component has its own contribution to the data quality.

ACKNOWLEDGEMENTS

The authors wish to acknowledge assistance provided through ANLEC R&D, supported by Low Emission Technology Australia (LETA) and the Australian Government through the Department of Industry, Science, Energy and Resources; the Victorian Government, BHP, the Commonwealth Government via the EIF and the CO2CRC members who have committed their time and support to the Stage 3 Project. CO2CRC wish to acknowledge the Otway International Test Centre landowners, community, Moyne Shire Council and regulatory bodies who have supported the site over the past decade of operation. We would like to acknowledge Ludovic Ricard for the help with the DTS dataset. Evgenii Sidenko is grateful to Professor Claus Otto and The Curtin University Oil and Gas Innovation Centre for providing the PhD stipend. Also, we would like to thank Julia Correa for the idea for this study. Special thanks to Professor Boris Gurevich (Curtin University) for his useful advice and the help with the manuscript preparation.

REFERENCES

- Adamovsky, G., S. F. Lyuksyutov, J. R. MacKey, B. M. Floyd, U. Abeywickrema, I. Fedin, and M. Rackaitis, 2012, Peculiarities of thermo-optic coefficient under different temperature regimes in optical fibers containing fiber Bragg gratings: *Optics Communications*, **285**, 766–773.
- Ajo-Franklin, J. B., S. Dou, N. J. Lindsey, I. Monga, C. Tracy, M. Robertson, V. Rodriguez Tribaldos, C. Ulrich, B. Freifeld, T. Daley, and X. Li, 2019, Distributed Acoustic Sensing Using Dark Fiber for Near-Surface Characterization and Broadband Seismic Event Detection: *Scientific Reports*, **9**, 1–14.
- Bakku*, S. K., M. Fehler, P. Wills, J. Mestayer, A. Mateeva, and J. Lopez, 2014, Vertical seismic profiling using distributed acoustic sensing in a hydrofrac treatment well: SEG Technical Program Expanded Abstracts 2014, 5024–5028.
- Bakku, S. K., 2015, Fracture Characterization from Seismic Measurements in a Borehole. Massachusetts Institute of Technology, 227p.
- Bao, X., and Y. Wang, 2021, Recent Advancements in Rayleigh Scattering-Based Distributed

Fiber Sensors: Advanced Devices & Instrumentation, **2021**, 1–17.

Becker, M., T. Coleman, C. Ciervo, M. Cole, and M. Mondanos, 2017, Fluid pressure sensing with fiber-optic distributed acoustic sensing: The Leading Edge, **36**, 1018–1023.

Becker, M. W., and T. I. Coleman, 2019, Distributed acoustic sensing of strain at earth tide frequencies: Sensors (Switzerland), **19**.

Becker, M. W., C. Ciervo, and T. Coleman, 2019, Laboratory testing of low frequency strain measured by distributed acoustic sensing: 2018 SEG International Exposition and Annual Meeting, SEG 2018, 4963–4966.

Bromirski, P. D., 2002, The near-coastal microseism spectrum: Spatial and temporal wave climate relationships: Journal of Geophysical Research, **107**, 2166.

Cook, P., 2014, Geologically Storing Carbon: Learning from the Otway Project Experience.: CSIRO PUBLISHING.

Fang, Z., K. K. Chin, R. Qu, and H. Cai, 2012, Fundamentals of Optical Fiber Sensors: John Wiley & Sons, Inc.

Feng, X., C. Sun, X. Zhang, and F. Ansari, 2010, Determination of the coefficient of thermal

expansion with embedded long-gauge fiber optic sensors: *Measurement Science and Technology*, **21**, 065302.

Feo, G., J. Sharma, D. Kortukov, W. Williams, and T. Ogunsanwo, 2020, Distributed fiber optic sensing for real-time monitoring of gas in riser during offshore drilling: *Sensors (Switzerland)*, **20**.

Freedman, D., R. Pisani, and R. Purves, 2007, *Statistics.*, 4th ed.: Norton.

Gao, H., Y. Jiang, Y. Cui, L. Zhang, J. Jia, and L. Jiang, 2018, Investigation on the thermo-optic coefficient of silica fiber within a wide temperature range: *Journal of Lightwave Technology*, **36**, 5881–5886.

Glubokovskikh, S., R. Pevzner, E. Sidenko, K. Tertyshnikov, B. Gurevich, S. Shatalin, A. Slunyaev, and E. Pelinovsky, 2021, Downhole distributed acoustic sensing provides insights into the structure of short-period ocean-generated seismic wavefield: *Journal of Geophysical Research: Solid Earth*, 1–28.

Isaenkov, R., R. Pevzner, S. Glubokovskikh, S. Yavuz, A. Yurikov, K. Tertyshnikov, B. Gurevich, J. Correa, T. Wood, B. Freifeld, M. Mondanos, S. Nikolov, and P. Barraclough,

2021, An automated system for continuous monitoring of CO₂ geosequestration using multi-well offset VSP with permanent seismic sources and receivers: Stage 3 of the CO₂CRC Otway Project: *International Journal of Greenhouse Gas Control*, **108**, 103317.

Jenkins, C., S. Marshall, T. Dance, J. Ennis-King, S. Glubokovskikh, B. Gurevich, T. La Force,

L. Paterson, R. Pevzner, E. Tenthorey, and M. Watson, 2017, Validating Subsurface Monitoring as an Alternative Option to Surface M&V - The CO₂CRC's Otway Stage 3 Injection: *Energy Procedia*, **114**, 3374–3384.

Jin, G., and B. Roy, 2017, Hydraulic-fracture geometry characterization using low-frequency

DAS signal: *The Leading Edge*, **36**, 975–980.

Karrenbach, M., A. Ridge, S. Cole, K. Boone, J. Rich, K. Silver, and D. Langton, 2017, DAS

Microseismic Monitoring and Integration With Strain Measurements in Hydraulic Fracture Profiling: *Proceedings of the 5th Unconventional Resources Technology Conference*, 1–3.

Karrenbach, M., S. Cole, A. Ridge, K. Boone, D. Kahn, J. Rich, K. Silver, and D. Langton, 2019,

Fiber-optic distributed acoustic sensing of microseismicity, strain and temperature during hydraulic fracturing: *GEOPHYSICS*, **84**, D11–D23.

- Koyamada, Y., M. Imahama, K. Kubota, and K. Hogari, 2009, Fiber-Optic Distributed Strain and Temperature Sensing With Very High Measurand Resolution Over Long Range Using Coherent OTDR: *Journal of Lightwave Technology*, **27**, 1142–1146.
- Lindsey, N. J., T. Craig Dawe, and J. B. Ajo-Franklin, 2019, Illuminating seafloor faults and ocean dynamics with dark fiber distributed acoustic sensing: *Science*, **366**, 1103–1107.
- Mateeva, A., J. Lopez, H. Potters, J. Mestayer, B. Cox, D. Kiyashchenko, P. Wills, S. Grandi, K. Hornman, B. Kuvshinov, W. Berlang, Z. Yang, and R. Detomo, 2014, Distributed acoustic sensing for reservoir monitoring with vertical seismic profiling: *Geophysical Prospecting*, **62**, 679–692.
- Miller, D. E., and T. Coleman, 2018, DAS and DTS at BradyHot Springs: Observations about Coupling and Coupled Interpretations: *Stanford Geothermal Workshop*, 1–13.
- Nishida, K., 2017, Ambient seismic wave field: *Proceedings of the Japan Academy, Series B*, **93**, 423–448.
- Palik, E. D., 1997, *Handbook of Optical Constants of Solids : Five-Volume Set : Handbook of Thermo-Optic Coefficients of Optical Materials with Applications* (G. C. Ghosh, ed.):

Burlington : Elsevier Science.

Raab, T. ., T. . Reinsch, S. R. Aldaz Cifuentes, and J. . Hennings, 2019, Real-Time Well-

Integrity Monitoring Using Fiber-Optic Distributed Acoustic Sensing: SPE Journal, **24**,

1997–2009.

Ricard, L., R. Pevzner, E. Sidenko, K. Tertyshnikov, S. Sharma, D. Van Gent, and R. Isaenkov,

2019, Transforming an abandoned well into a permanent downhole receiver array: Harvey-3

case study: ASEG Extended Abstracts, **2019**, 1–4.

Roy, R., D. K. Agrawal, and H. A. McKinstry, 1989, Very Low Thermal Expansion Coefficient

Materials: Annual Review of Materials Science, **19**, 59–81.

Sharma, J., T. Cuny, O. Ogunsanwo, and O. Santos, 2021, Low-Frequency Distributed Acoustic

Sensing for Early Gas Detection in a Wellbore: IEEE Sensors Journal, **21**, 6158–6169.

Sharma, J., O. L. A. Santos, G. Feo, O. Ogunsanwo, and W. Williams, 2020, Well-scale

multiphase flow characterization and validation using distributed fiber-optic sensors for gas

kick monitoring: Optics Express, **28**, 38773.

Titov, A., Y. Fan, G. Jin, A. Tura, K. Kutun, and J. Miskimins, 2020, Experimental Investigation

of Distributed Acoustic Fiber-Optic Sensing in Production Logging: Thermal Slug Tracking and Multiphase Flow Characterization: Day 4 Thu, October 29, 2020.

Wang, H. F., X. Zeng, D. E. Miller, D. Fratta, K. L. Feigl, C. H. Thurber, and R. J. Mellors, 2018, Ground motion response to an ML 4.3 earthquake using co-located distributed acoustic sensing and seismometer arrays: *Geophysical Journal International*, **213**, 2020–2036.

LIST OF FIGURES

Figure 1. Schematic of NGL well experiment.

Figure 2. DTS and DAS response to the temperature change in the Curtin/NGL well. (a) - DTS response after temperature baseline subtraction, (b) - DTS time derivative, (c) – DAS strain-rate response.

Figure 3. DTS and DAS before and after common-mode noise removal. Common-mode noise is indicated by black arrows. Red arrows indicate DAS strain-rate response to the

temperature change. (a) – DTS signal at 26 m depth before and after common-mode noise removal; (b) – DAS signal at 26 m depth before and after common-mode noise removal; (c) - DTS signal at 847 m depth before and after common-mode noise removal; (d) – DAS signal at 847 m depth before and after common-mode noise removal.

Figure 4. DAS strain-rate response (common-mode noise) to changing room temperature.

(a) – DAS signal in the NGL well; (b) – DAS averaged signal and temperature recorded in the acquisition room.

Figure 5. Ice response on DAS data. (a) – the whole well interval before the common-mode noise removal; (b) – first 100 m of the well before the common-mode noise removal; (c) – first 100 m of the well after the common-mode noise removal. Dashed line in (a) shows the depth interval used to estimate the DAS common-mode noise.

Figure 6. Comparison of DAS and DTS responses. (a) – DAS strain rate response (black curve) and time derivative of temperature/DTS (orange curve); (b) - strain (black curve) calculated from DAS strain rate and DTS response (blue curve).

Figure 7. Schematic of the laboratory setup for DAS temperature test.

Figure 8. Laboratory test on a bare fiber: (a) - DAS strain-rate response over all channels; (b) - DAS averaged strain-rate trace (black curve) and temperature time derivative (orange curve); (c) - DAS converted to strain (black curve) and temperature log (orange curve).

Figure 9. Laboratory test on a tight-buffered fiber: (a) - DAS strain-rate response over all channels; (b) - DAS averaged strain-rate trace (black curve) and temperature time derivative (orange curve); (c) - DAS converted to strain (black curve) and temperature log (orange curve).

Figure 10. Otway site map. Black lines show projections of monitoring wells' trajectories (CRC 4, 5, 6, 7) on the surface. CRC3 well is a subvertical injection well.

Figure 11. Schematic of the configuration of borehole fiber-optic monitoring equipment in the CRC-6 and CRC-7 wells.

Figure 12. DAS and pressure-temperature gauges responses to water injections in the CRC6 and CRC7 wells. (a, b) - Pressure and temperature gauge responses in the CRC-6 and CRC-7 wells; (c, d) - spectrograms showing low-frequency strain-rate response from water injections in the CRC-6 and CRC-7 wells.

Figure 13. DTS and DAS data recorded during water injection in the CRC-6 well. Plot “a” shows DTS data recorded in the CRC-6 well; plot “b” shows DAS data recorded in the CRC-7 well; plots “c” and “d” show CRC-6 DAS data before and after signal compensation.

Figure 14. DTS and DAS data recorded during water injection in the CRC-5 well. Plot “a” shows DTS data recorded in the CRC-5 well; plot “b” shows DAS data recorded along the surface part of the DAS cable; plots “c” and “d” show CRC-5 DAS data before and after signal compensation.

Figure 15. Cross-plots between DAS strain and temperature change for NGL well and laboratory experiment: (a) – NGL well (“ice” level, 26 m); (b) – bare fiber in water bath (averaged); (c) – tight-buffered fiber in water bath (averaged).

Figure 16. Strain-temperature crossplots between DAS and DTS data recorded during water injections at Otway site. Black plots show relation between temperature change and strain before compensation of acquisition noise; blue plots shows data after compensation of the acquisition noise. (a,b) – water injection in CRC-4; (c,d) –water injection in CRC-5; (e,f) –water injection in CRC-6; (g,h) –water injection in CRC-7.

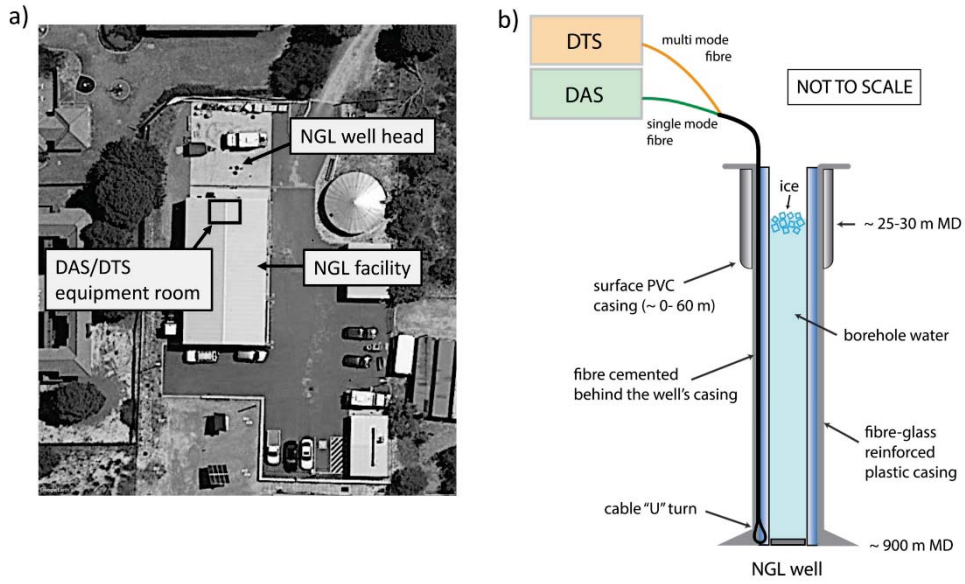


Figure 1. Schematic of NGL well experiment.

265x161mm (600 x 600 DPI)

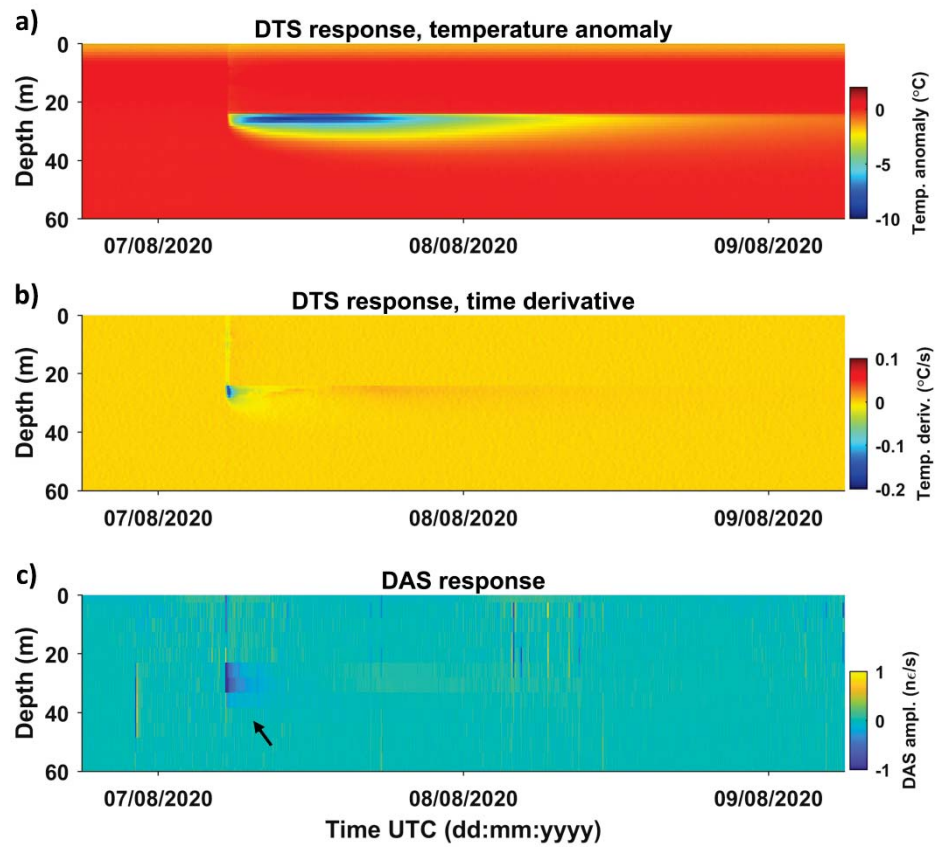


Figure 2. DTS and DAS response to the temperature change in the Curtin/NGL well. (a) - DTS response after temperature baseline subtraction, (b) - DTS time derivative, (c) - DAS strain-rate response.

192x175mm (600 x 600 DPI)

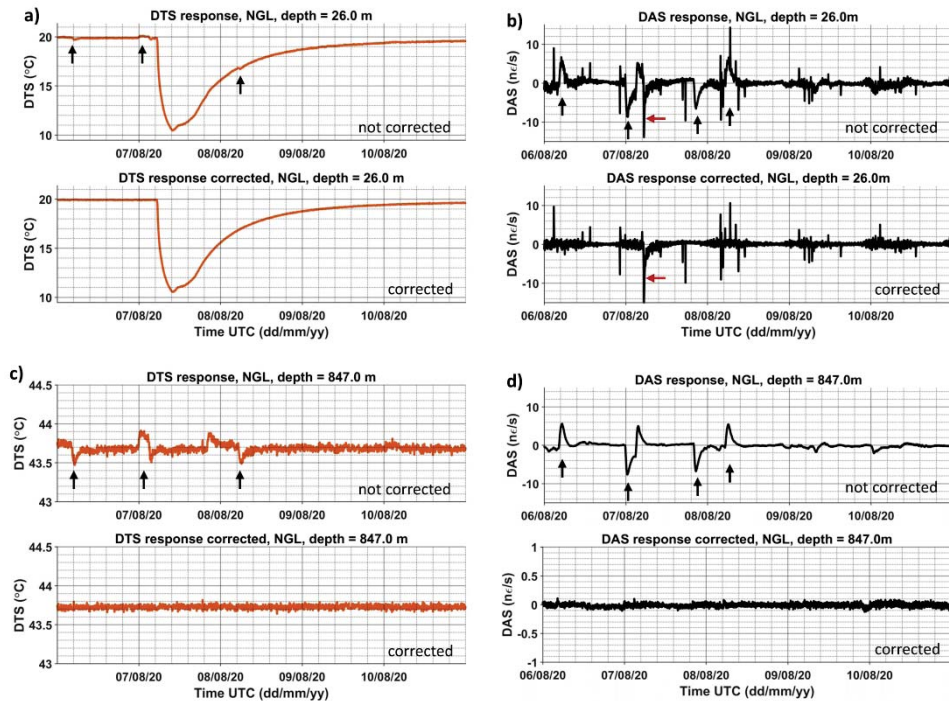


Figure 3. DTS and DAS before and after common-mode noise removal. Common-mode noise is indicated by black arrows. Red arrows indicate DAS strain-rate response to the temperature change. (a) – DTS signal at 26 m depth before and after common-mode noise removal; (b) – DAS signal at 26 m depth before and after common-mode noise removal; (c) - DTS signal at 847 m depth before and after common-mode noise removal; (d) – DAS signal at 847 m depth before and after common-mode noise removal.

251x185mm (600 x 600 DPI)

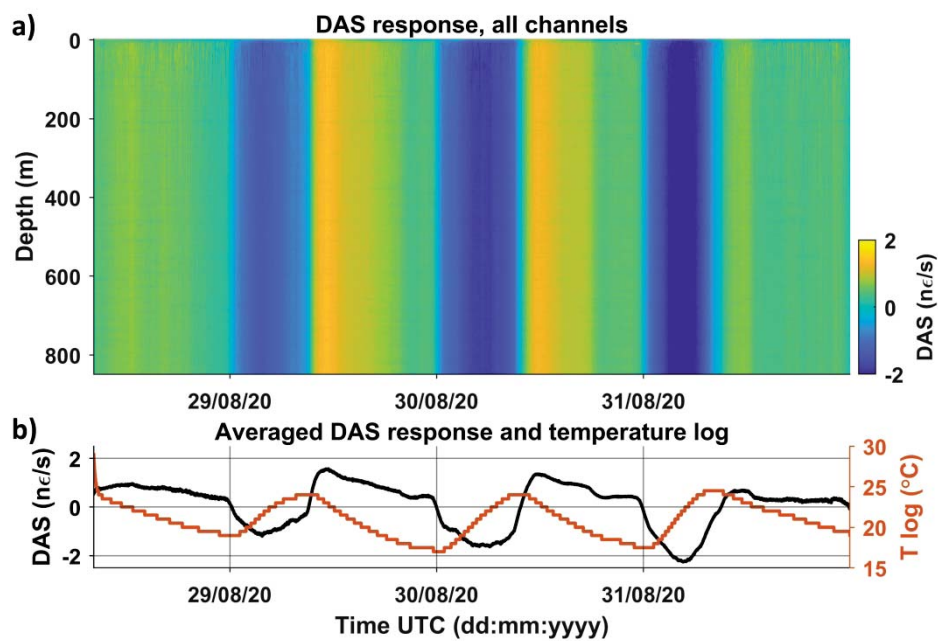


Figure 4. DAS strain-rate response (common-mode noise) to changing room temperature. (a) – DAS signal in the NGL well; (b) – DAS averaged signal and temperature recorded in the acquisition room.

230x158mm (600 x 600 DPI)

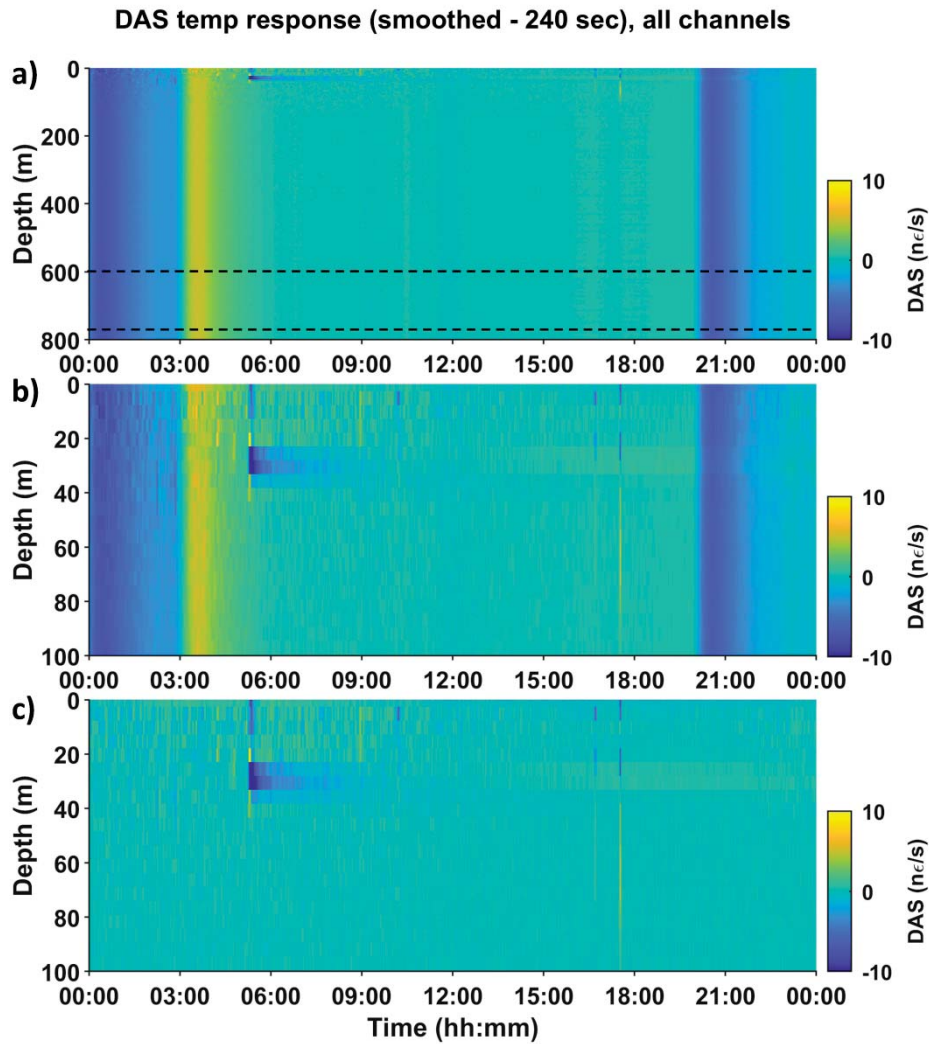


Figure 5. Ice response on DAS data. (a) – the whole well interval before the common-mode noise removal; (b) – first 100 m of the well before the common-mode noise removal; (c) – first 100 m of the well after the common-mode noise removal. Dashed line in (a) shows the depth interval used to estimate the DAS common-mode noise.

169x184mm (600 x 600 DPI)

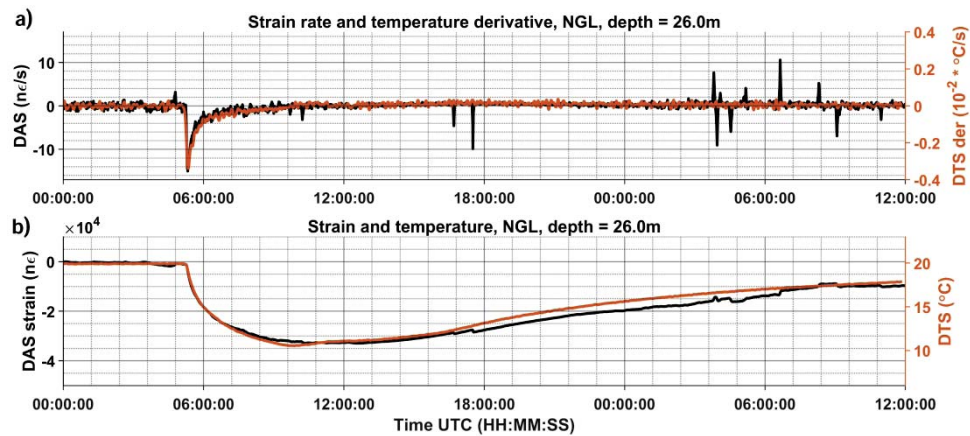


Figure 6. Comparison of DAS and DTS responses. (a) – DAS strain rate response (black curve) and time derivative of temperature/DTS (orange curve); (b) - strain (black curve) calculated from DAS strain rate and DTS response (blue curve).

281x131mm (600 x 600 DPI)

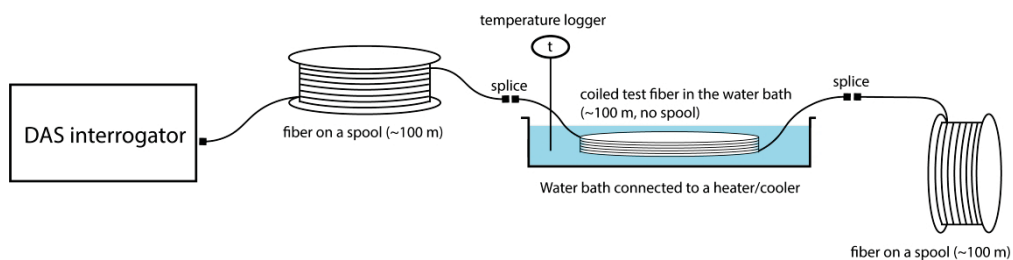


Figure 7. Schematic of the laboratory setup for DAS temperature test.

229x57mm (600 x 600 DPI)

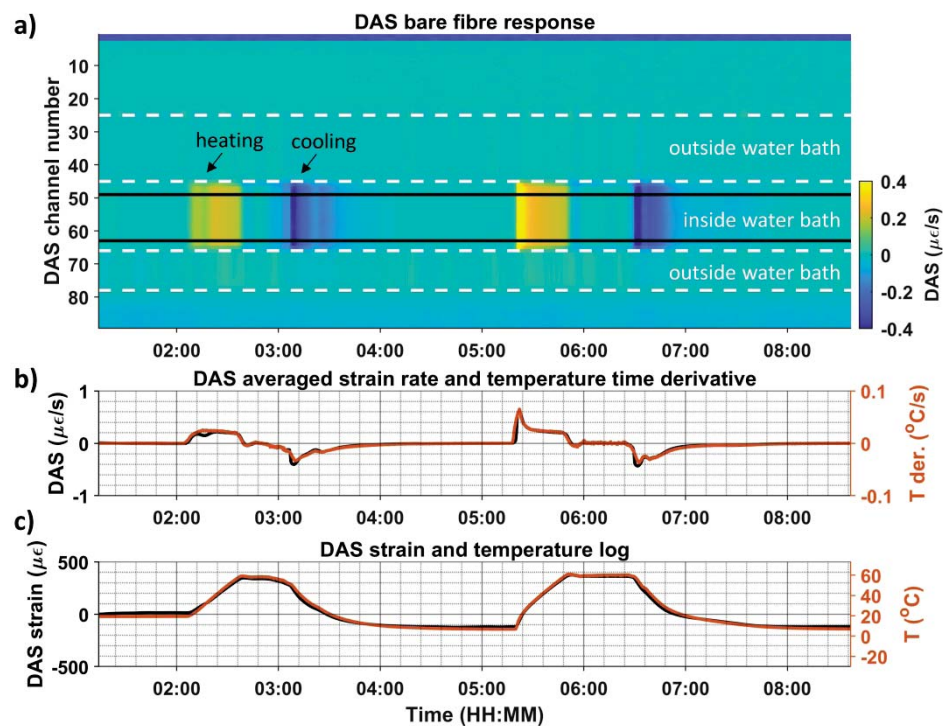


Figure 8. Laboratory test on a bare fiber: (a) - DAS strain-rate response over all channels; (b) - DAS averaged strain-rate trace (black curve) and temperature time derivative (orange curve); (c) - DAS converted to strain (black curve) and temperature log (orange curve).

221x172mm (600 x 600 DPI)

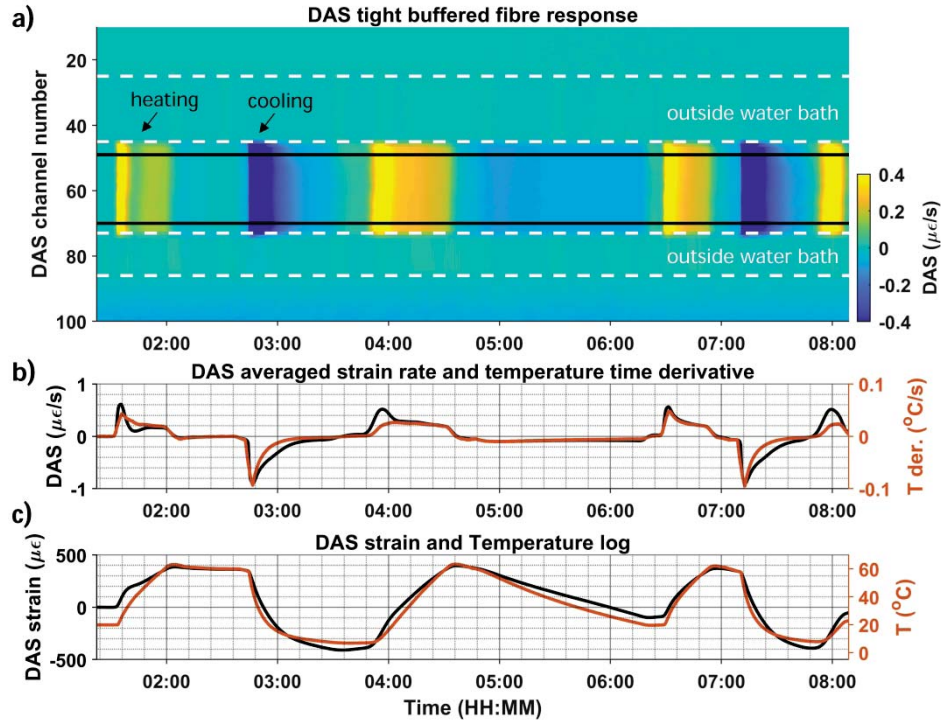


Figure 9. Laboratory test on a tight-buffered fiber: (a) - DAS strain-rate response over all channels; (b) - DAS averaged strain-rate trace (black curve) and temperature time derivative (orange curve); (c) - DAS converted to strain (black curve) and temperature log (orange curve).

221x172mm (600 x 600 DPI)

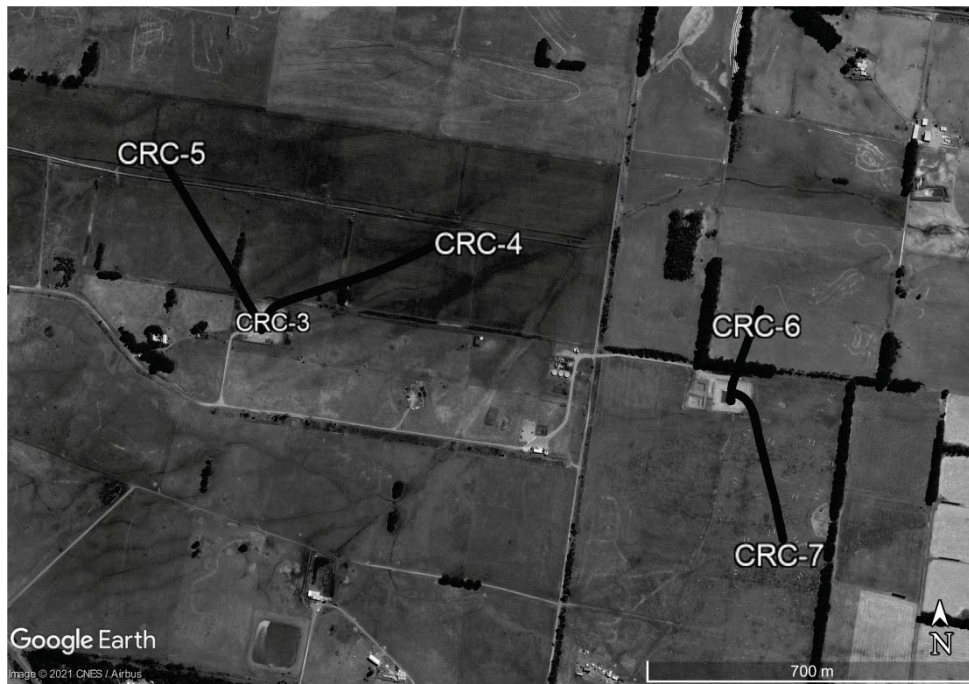


Figure 10. Otway site map. Black lines show projections of monitoring wells' trajectories (CRC 4, 5, 6, 7) on the surface. CRC3 well is a subvertical injection well.

297x209mm (600 x 600 DPI)

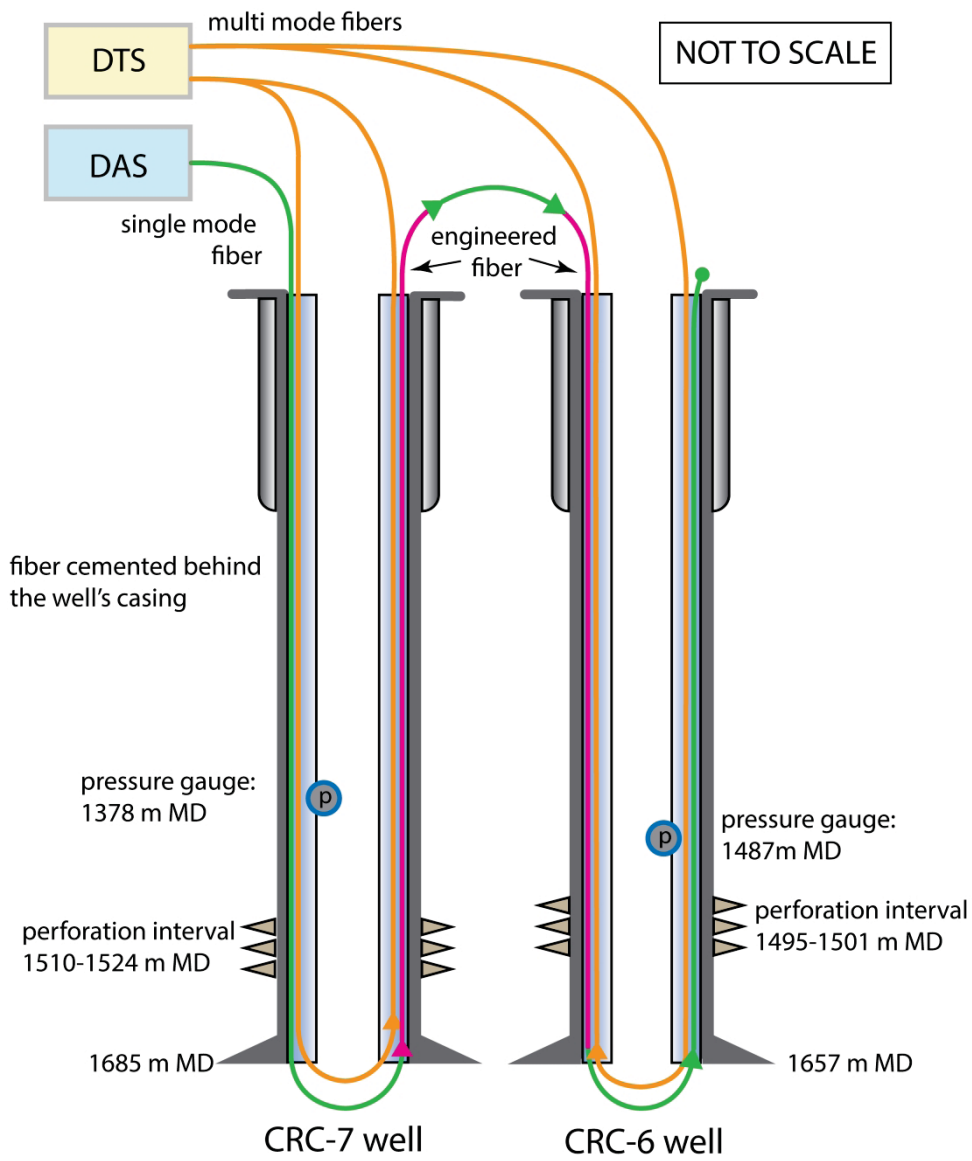


Figure 11. Schematic of the configuration of borehole fiber-optic monitoring equipment in the CRC-6 and CRC-7 wells.

147x170mm (600 x 600 DPI)

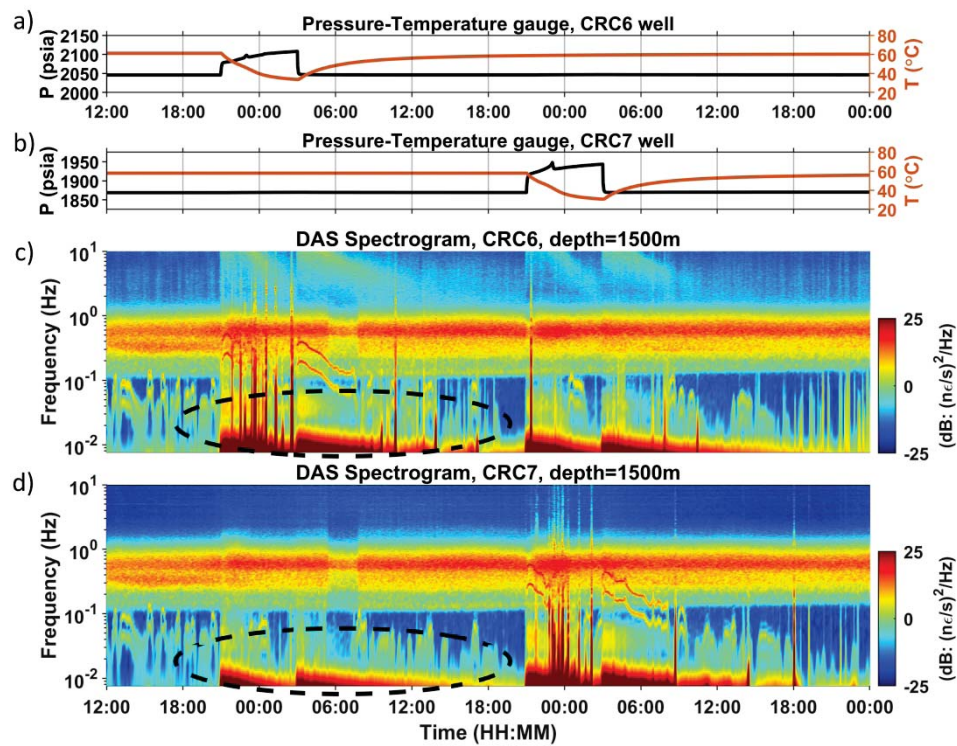


Figure 12. DAS and pressure-temperature gauges responses to water injections in the CRC6 and CRC7 wells. (a, b) - Pressure and temperature gauge responses in the CRC-6 and CRC-7 wells; (c, d) - spectrograms showing low-frequency strain-rate response from water injections in the CRC-6 and CRC-7 wells.

181x141mm (600 x 600 DPI)

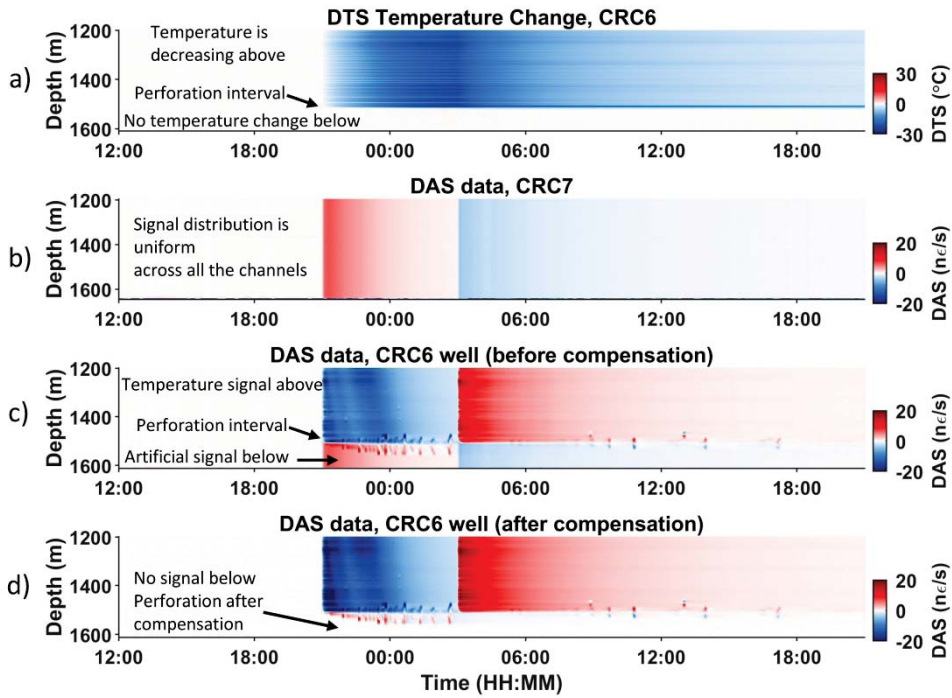


Figure 13. DTS and DAS data recorded during water injection in the CRC-6 well. Plot "a" shows DTS data recorded in the CRC-6 well; plot "b" shows DAS data recorded in the CRC-7 well; plots "c" and "d" show CRC-6 DAS data before and after signal compensation.

194x141mm (600 x 600 DPI)

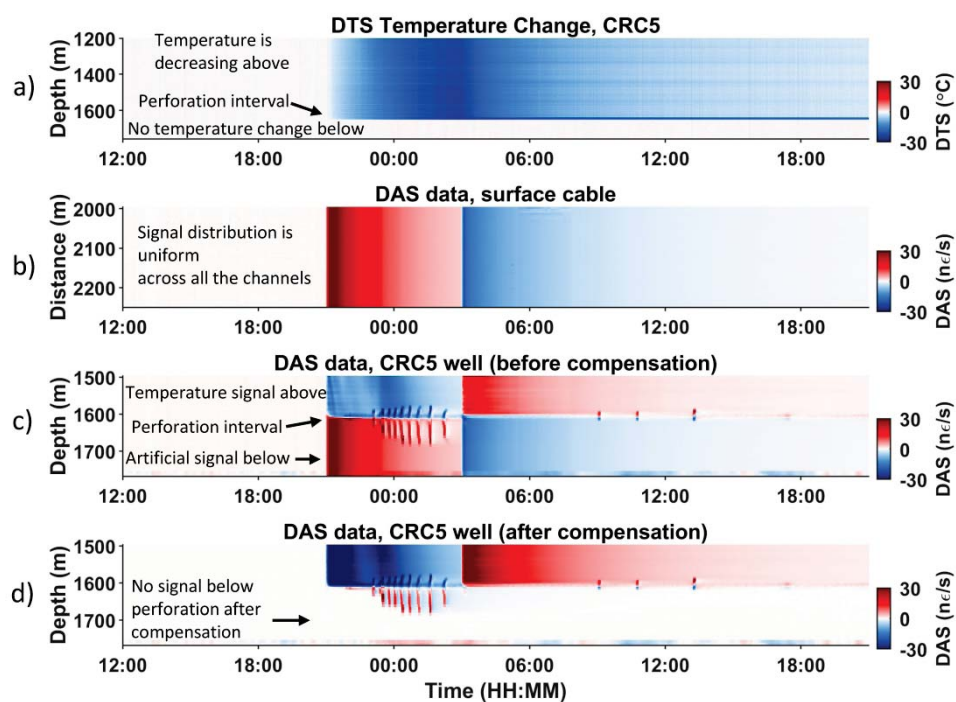


Figure 14. DTS and DAS data recorded during water injection in the CRC-5 well. Plot "a" shows DTS data recorded in the CRC-5 well; plot "b" shows DAS data recorded along the surface part of the DAS cable; plots "c" and "d" show CRC-5 DAS data before and after signal compensation.

194x141mm (600 x 600 DPI)

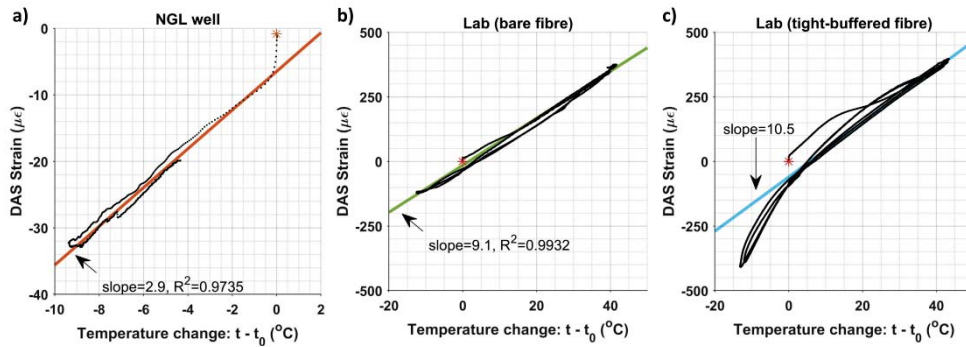


Figure 15. Cross-plots between DAS strain and temperature change for NGL well and laboratory experiment: (a) – NGL well (“ice” level, 26 m); (b) – bare fiber in water bath (averaged); (c) – tight-buffered fiber in water bath (averaged).

278x99mm (600 x 600 DPI)

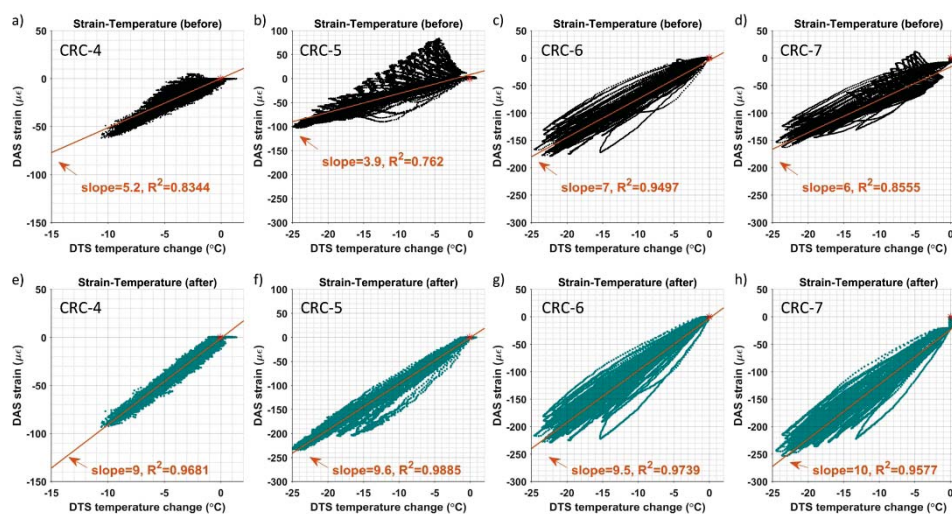


Figure 16. Strain-temperature crossplots between DAS and DTS data recorded during water injections at Otway site. Black plots show relation between temperature change and strain before compensation of acquisition noise; blue plots shows data after compensation of the acquisition noise. (a,b) – water injection in CRC-4; (c,d) –water injection in CRC-5; (e,f) –water injection in CRC-6; (g,h) –water injection in CRC-7.

181x98mm (600 x 600 DPI)

DATA AND MATERIALS AVAILABILITY

Custom statement of data and materials availability